The Journal of Chemical Physics

RESEARCH ARTICLE | JUNE 08 2023

Exploring the distinct conformational preferences of allyl ethyl ether and allyl ethyl sulfide using rotational spectroscopy and computational chemistry

Tamanna Poonia ; Jennifer van Wijngaarden

J. Chem. Phys. 158, 224301 (2023)
https://doi.org/10.1063/5.0153479

The Journal of Chemical Physics ARTICLE scitation.org/journal/jcp

Exploring the distinct conformational preferences of allyl ethyl ether and allyl ethyl sulfide using rotational spectroscopy and computational chemistry

Cite as: J. Chem. Phys. 158, 224301 (2023); doi: 10.1063/5.0153479
Submitted: 8 April 2023 • Accepted: 18 May 2023 •
Published Online: 8 June 2023

Tamanna Poonia[1] and Jennifer van Wijngaarden[1,2,a)]

AFFILIATIONS

[1] Department of Chemistry, University of Manitoba, Winnipeg, Manitoba R3T 2N2, Canada
[2] Department of Chemistry, York University, Toronto, Ontario M3J 1P3, Canada

[a)] **Author to whom correspondence should be addressed:** vanwijng@yorku.ca

ABSTRACT

The conformational energy landscapes of allyl ethyl ether (AEE) and allyl ethyl sulfide (AES) were investigated using Fourier transform microwave spectroscopy in the frequency range of 5–23 GHz aided by density functional theory B3LYP-D3(BJ)/aug-cc-pVTZ calculations. The latter predicted highly competitive equilibria for both species, including 14 unique conformers of AEE and 12 for the sulfur analog AES within 14 kJ mol^{-1}. The experimental rotational spectrum of AEE was dominated by transitions arising from its three lowest energy conformers, which differ in the arrangement of the allyl side chain, while in AES, transitions due to the two most stable forms, distinct in the orientation of the ethyl group, were observed. Splitting patterns attributed to methyl internal rotation were analyzed for AEE conformers I and II, and the corresponding V_3 barriers were determined to be 12.172(55) and 12.373(32) kJ mol^{-1}, respectively. The experimental ground state geometries of both AEE and AES were derived using the observed rotational spectra of the ^{13}C and ^{34}S isotopic species and are highly dependent on the electronic properties of the linking chalcogen (oxygen vs sulfur). The observed structures are consistent with a decrease in hybridization in the bridging atom from oxygen to sulfur. The molecular-level phenomena that drive the conformational preferences are rationalized through natural bond orbital and non-covalent interaction analyses. These show that interactions involving the lone pairs on the chalcogen atom with the organic side chains favor distinct geometries and energy orderings for the conformers of AEE and AES.

INTRODUCTION

Chalcogen substitution has garnered attention in the materials science[1] and polymer electronics communities[1–5] as a way to tune the physical and chemical properties of sensors,[6] light emitting devices,[7] transistors,[8] and photovoltaics.[9] When a heavier chalcogen atom replaces a lighter one, the electronic structure is sensitively affected by the differences in atomic size, polarizability, and electronegativity, which alter molecular-level interactions and, consequently, the bulk and surface properties of the material.[1,10–13] A subclass of these materials is organochalcogens, compounds having a group 6 element covalently bonded to an organic fragment, with applications across chemistry and biochemistry.[14–20] From a fundamental point of view, these systems serve as excellent prototypes to explore the intramolecular interactions between chalcogen atoms and organic frameworks as the lone pairs on the former can stabilize multiple arrangements of the latter. Rotational spectroscopy combined with quantum chemical calculations provides sensitive and detailed information about the underlying potential energy surfaces that govern such conformational distributions in monomers[21–23] and molecular complexes.[24,25] As conformationally specific processes play a pivotal role in the selectivity and function of chemical and biochemical reactions,[26–30] a further understanding of the factors that define conformational space in organochalcogens may lead to improved design and tunability of these materials.

In *n*-alkane substituted alcohols and thiols, computational models predict that the chalcogen strongly influences the conformational arrangement (even as far as three dihedral angles away) and that sulfur-containing species have more energetically distinct conformers.[31] This has been experimentally verified in ethanethiol,[32] 1-propanethiol,[33] and 1-butanethiol,[34] for which rotational spectroscopic measurements confirmed that the most stable conformers have a *gauche* arrangement of the CCSH fragment, whereas in the oxygen analogs,[34–37] the lowest energy conformers slightly favor *trans* CCOH orientations (sometimes by only a few tenths of kJ mol^{-1}). While Vansteenkiste *et al.*[31] predicted that n-alkane substituted ethers also present much more competitive equilibria than their sulfur counterparts, establishing a general rule for the conformational preferences of ethers vs sulfides is less tractable because of the complexity in isolating the effects of the two organic fragments.

A recent microwave spectroscopic study of the chalcogen-bridged compounds diallyl sulfide (DAS) and diallyl ether (DAE)[38] confirmed that the sulfur compound does give rise to more energetically distinct conformers even when the organic substituent is partially unsaturated, as rotational transitions for nine low energy (<3 kJ mol^{-1}) conformers for DAE and only one conformer for DAS were observed under analogous experimental conditions. The accompanying quantum chemical calculations revealed that the numerous DAE conformers were stabilized by hyperconjugative interactions involving the lone pairs on oxygen shared with the allyl side chains, which were absent in DAS despite a similar arrangement of the allyl side chains. This finding is consistent with the geometry at the central atom (C–X–C angle), which is ~14° larger in DAE than in sulfide due to the greater hybrid character of the bonding orbitals on oxygen. The prevalence of these stabilizing interactions in the ether was consequently reported to be the underlying cause of the competitive equilibrium of DAE (in comparison with DAS); however, the observation that the CCXC dihedral angles (where X = S or O) are gauche, regardless of the bridging atom identity, is an important distinction in comparison with earlier studies of alcohols and thiols having the chalcogen within the terminal functional group.

To investigate whether it is universally true that organic ethers adopt many more stable forms than their heavy congeners and that the conformational preferences are less unique than when the chalcogen is part of an end group, the present study targets the conformational equilibria of allyl ethyl ether (AEE) and allyl ethyl sulfide (AES). The replacement of one of the allyl side chains of DAE and DAS by a fully saturated ethyl group removes bilateral symmetry and provides a more direct comparison with the studies on n-alkane substituted organochalcogens.[31] It also introduces the possibility of observing effects due to methyl rotation, as has been reported for related compounds, such as allyl methyl ether[39] [conformer I, V_3 = 8.71(13) kJ mol^{-1}; conformer II, V_3 = 9.93(13) kJ mol^{-1}], allyl methyl sulfide[40] [V_3 = 7.41(34) kJ mol^{-1}], methyl vinyl ether[41] [V_3 = 16.03(42) kJ mol^{-1}], and ethyl vinyl ether[42] [V_3 = 12.85(10) kJ mol^{-1}].

In this article, the conformational equilibria of AEE and AES are reported for the first time using Fourier transform microwave (FTMW) spectroscopy aided by B3LYP-D3(BJ)/aug-cc-pVTZ calculations. The computational results predicted unique conformational landscapes for both species and were used to assign rotational transitions for three conformers of AEE and two conformers of AES. The experimental rotational constants of several isotopologues of conformers I of AEE and AES were then used to accurately derive their experimental substitution (r_s) and ground state effective (r_0) geometries. For conformers I and II of AEE, a splitting consistent with the methyl internal rotation was resolved sufficiently to derive experimental V_3 barriers that are in good agreement with theoretical estimates. Natural bond orbital (NBO)[43] and non-covalent interaction (NCI)[44] analyses provide insights into the molecular-level interactions that give rise to unique geometric forms in the conformational mixtures of AEE and AES.

EXPERIMENTAL METHODS

Commercial samples of AEE (95%, bp: 67 °C) from Sigma-Aldrich Canada and AES (97%, bp: 115–116 °C) from Alfa Aesar Canada were used without further purification. A gas mixture was prepared for each compound with ~1% AEE or AES diluted in neon (100–200 kPa) using the vapor pressure from the liquid samples at room temperature. To generate a supersonic jet, the gas mixtures were expanded through a pulsed nozzle (1 mm diameter) into the high vacuum chambers of the spectrometers. The rotational spectra of AEE and AES were then obtained using both chirped-pulse (cp)[45] and Balle–Flygare (BF)[46] FTMW instruments, which were previously described in detail.[47,48] Initially, a survey cp-FTMW spectrum of each compound was collected in the frequency range of 8–18 GHz in segments of 2 GHz each and used to assign the most intense transitions of the conformers of AEE and AES. Later, on the basis of the survey spectrum, final frequency measurements were done using the higher resolution, higher sensitivity BF-FTMW spectrometer from 5 to 23 GHz. The collinear arrangement of the resonator axis and the molecular beam in the BF-FTMW spectrometer creates a Doppler splitting of the observed transitions, and the transition frequency is taken as the arithmetic mean of the doublet. With this instrument, rotational transitions have line widths of ~7 kHz (FWHM) and the uncertainty in measuring line positions is typically 2 kHz.

COMPUTATIONAL METHODS

The arrangement of the heavy atoms of the organic side chains is described by three dihedral angles θ, ϕ, and λ (defined in Fig. 1) and gives rise to the various conformers of AEE and AES. Initially, a conformational search was performed using the Conformer–Rotamer Ensemble Sample Tool (CREST) at the GFN2-xTB[49] level of theory making use of extended tight binding (xTB).[50,51] The conformational search identified 34 and 44 possible molecular geometries for AEE and AES, respectively. Next, these potential geometries were optimized using dispersion-corrected density functional theory (DFT) at the B3LYP[52]-D3(BJ)[53,54]/aug-cc-pVTZ[55] level using the Gaussian 16 program.[56] To confirm the nature of the stationary points and to obtain electronic energies with zero-point energy (ZPE) corrections and quartic centrifugal distortion constants, harmonic frequency calculations were performed. To generate the interconversion pathways between conformers, relaxed potential energy curves were derived for both molecules at the same level of theory from a series of single point energy calculations involving a change in the dihedral angle of interest by 10°. In a similar manner, the methyl internal rotation barriers (V_3) were calculated and are plotted in Fig. 2 for conformers I and II of AEE. To

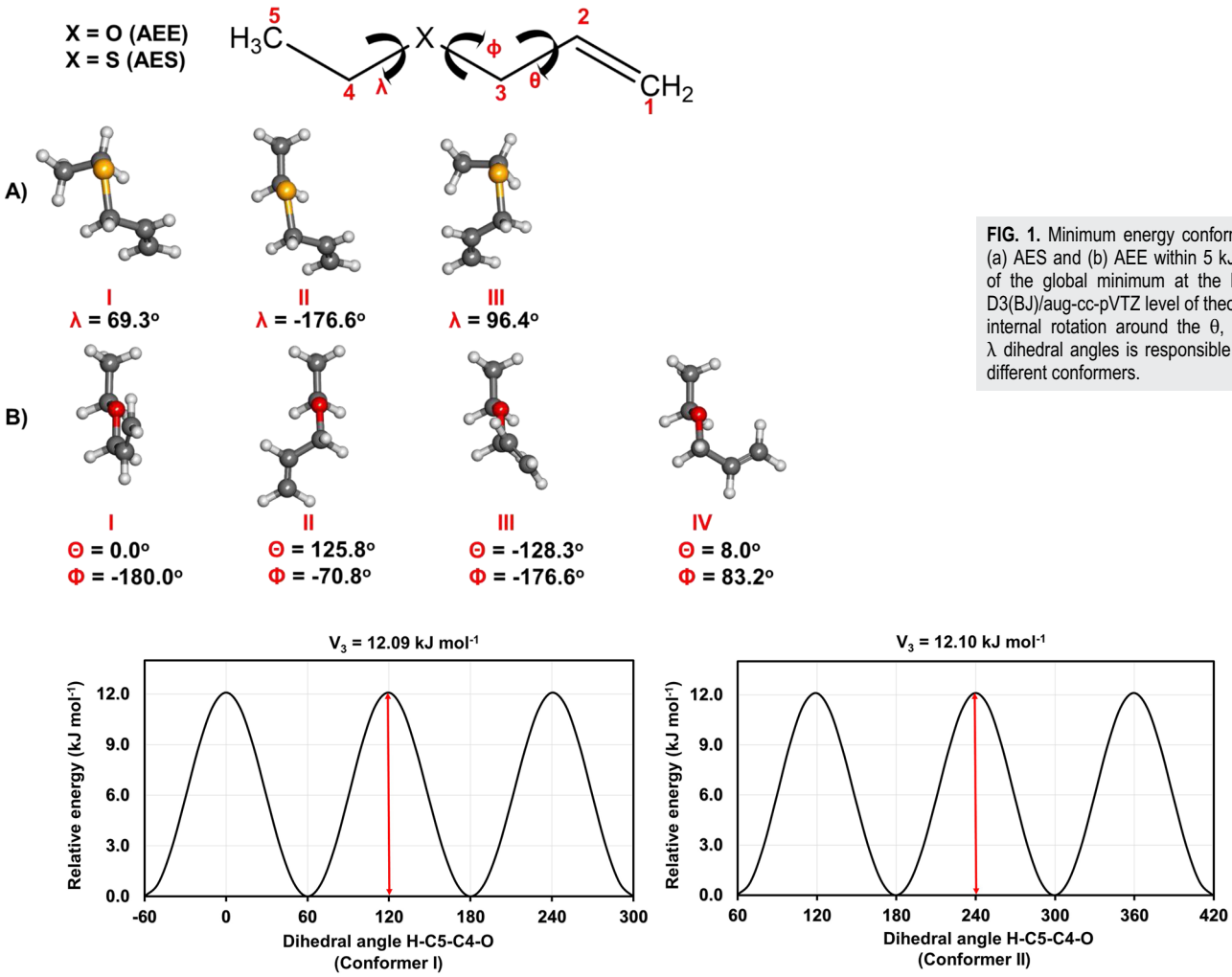

FIG. 1. Minimum energy conformers of (a) AES and (b) AEE within 5 kJ mol^{-1} of the global minimum at the B3LYP-D3(BJ)/aug-cc-pVTZ level of theory. The internal rotation around the θ, ϕ, and λ dihedral angles is responsible for the different conformers.

FIG. 2. Methyl internal rotation potential energy scan for AEE conformers I and II at the B3LYP-D3(BJ)/aug-cc-pVTZ level of theory. The analogous barrier in conformer III was found to be 11.97, and it was 11.20 and 11.84 kJ mol^{-1} in conformers I and II of AES, respectively.

investigate intra- and intermolecular contacts, non-covalent interaction (NCI)[44] and natural bond orbital (NBO)[43] calculations were done using the NCIPLOT[57] and NBO 7.0[58] programs, respectively.

RESULTS

Conformational space of AEE and AES

A surprisingly rich conformational space was identified for both AEE and AES, as geometry optimization calculations identified 14 unique conformers for AEE within 13.4 kJ mol^{-1} and 12 for AES within 13 kJ mol^{-1}. The Cartesian coordinates of all conformers of AES and AEE are summarized in the ESI (Electronic Supplementary Material File) in Tables S1–S26. Their calculated energetic and spectroscopic parameters at the B3LYP-D3(BJ)/aug-cc-pVTZ level of theory are given in Table I. As high energy conformers are not anticipated to be sufficiently populated at room temperature to persist in the supersonic jet for microwave spectroscopic detection, only conformers with relative energies within 5 kJ mol^{-1} of the global minimum were considered further and these geometries are shown in Fig. 1 for both compounds. The labeling of conformers was done using Roman numerals to describe their stability ordering, where conformer I is the most stable conformer (relative energy set to zero).

Spectral analysis

The theoretical results (Table I) were used to simulate the rotational spectra of the low-energy forms of AEE and AES for comparison with the experimental data. From this, transitions due to three near prolate top conformers of AEE and two conformers of AES were assigned in the cp-FTMW spectrum. For the ground states

TABLE I. Calculated energetic and spectroscopic parameters for the conformers of AES and AEE at the B3LYP-D3(BJ)/aug-cc-pVTZ level of theory.

AES	ΔE_0[a]	P[b]	A/B/C[c]	$\lvert\mu_a\rvert/\lvert\mu_b\rvert/\lvert\mu_c\rvert$[d]
I	0.0	55.8	3667/2049/1531	0.5/1.3/0.2
II	2.2	23.1	4792/1626/1312	0.5/1.2/0.6
III	4.6	8.9	3518/2140/1499	0.8/1.1/0.7
IV	7.6	2.6	6998/1309/1199	0.7/1.3/0.9
V	8.2	2.0	4166/1794/1644	0.0/1.4/0.7
VI	8.3	1.9	7556/1275/1188	0.7/1.3/0.8
VII	8.8	1.6	4881/1576/1375	0.1/1.6/0.2
VIII	9.0	1.4	7193/1283/1190	0.0/1.2/1.0
IX	9.4	1.3	4944/1582/1317	0.5/1.2/1.1
X	10.8	0.7	3741/2087/1623	0.1/0.9/1.4
XI	12.8	0.3	7341/1404/1261	0.9/1.5/0.6
XII	13.0	0.3	9831/1267/1146	0.6/1.7/0.0
AEE	ΔE_0[a]	P[b]	A/B/C[c]	$\lvert\mu_a\rvert/\lvert\mu_b\rvert/\lvert\mu_c\rvert$[d]
I	0.0	31.7	9584/1712/1493	0.7/1.2/0.0
II	0.8	23.0	8502/1745/1582	0.5/0.9/0.5
III	1.3	18.8	15 000/1385/1346	0.3/1.1/0.0
IV	2.8	10.3	6998/2069/1761	0.1/0.2/1.2
V	5.4	3.6	10 237/1703/1602	1.1/1.1/0.4
VI	5.6	3.3	6169/2113/1845	0.3/1.2/0.1
VII	6.3	2.5	10 729/1572/1462	0.6/0.6/1.0
VIII	7.0	1.9	12 836/1487/1451	0.6/0.7/0.9
IX	7.3	1.7	7947/1966/1803	0.3/0.2/1.3
X	7.6	1.5	5434/2376/1886	0.5/0.8/0.8
XI	9.0	0.8	5621/2478/2027	0.5/0.1/1.3
XII	11.3	0.3	7988/1866/1629	0.5/0.6/1.1
XIII	11.4	0.3	11 737/1554/1534	0.3/0.2/1.3
XIV	13.4	0.1	6639/2031/1704	0.1/0.5/1.2

[a]Zero-point energy (ZPE) corrected relative energies in kJ mol^{-1}.
[b]Boltzmann population at 298 K in %.
[c]Rotational constants in MHz.
[d]Magnitude of the electric dipole moment components in Debye.

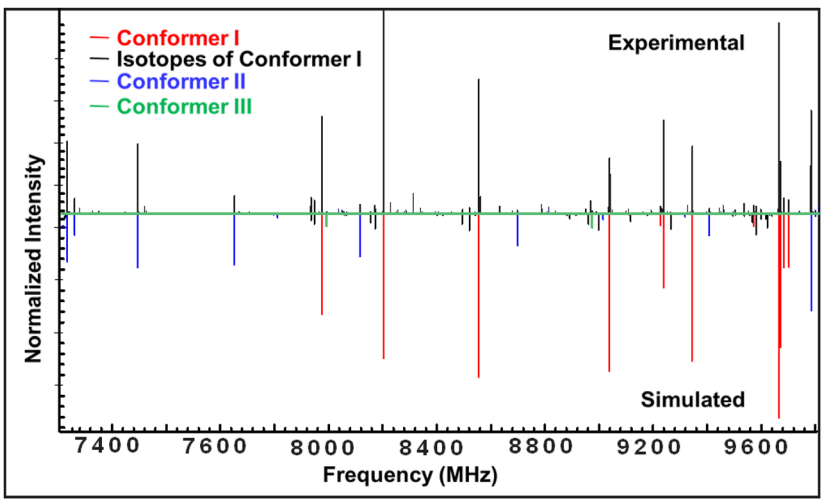

FIG. 3. Portion of the broadband cp-FTMW spectrum (1.5×10^6 free induction decays) of AEE for conformer I and its minor heavy atom isotopic species, plus those of conformers II and III. The top portion is the experimental spectrum, and the lower portion is the simulated spectrum using the fitted parameters.

(conformer 1) of AEE and AES, transitions due to all five ^{13}C isotopologues were also observed in natural abundance, as were those of the ^{34}S analog of AES with intensities of ~1% and ~4% of the corresponding parent lines, respectively. A portion of the broadband spectrum of AEE featuring transitions of the three assigned conformers is shown in Fig. 3, revealing spectral intensities that are qualitatively consistent with the predicted populations and dipole moments. A more quantitative analysis of the observed intensities, to confirm the conformer abundances, is challenging because of variations in instrument response across the spectral region and differences in spectroscopic constants such that comparable transitions have distinct energies. The initial assignments were confirmed using measurements from the BF-FTMW spectrometer, and additional transitions were recorded to extend the frequency coverage and augment the dataset with lower intensity features.

During higher resolution measurements of AEE, a splitting pattern was observed in some transitions of conformers I and II. These were readily resolved for 20 strong Q-branch *b*-type transitions of conformer II with $K_a' = 2$ and also for the R-branch *a*-type transitions (both conformers) and P-branch *b*-type transitions (conformer I) with $K_a' = 3$. Initially, we attempted to model the splitting as a tunneling motion involving a torsion of the allyl group as reported for allyl methyl amine,[21] but this was not consistent with the observed *c*-type transitions, which would need to connect the tunneling states (+/−) to create closed loops in the energy level diagram. In the end, the tunneling splitting was successfully treated as a methyl rotation with the individual components fit to the A/E states of the internal rotor. A sample spectrum is shown in Fig. 4. Although conformer III has a similar V_3 barrier for this motion, splitting was not observed in its spectrum. This was attributed to the fact that only the more intense $K_a = 0$ and 1 transitions were measured for this higher energy form. In conformers I and II, the analogous lower K_a transitions did not exhibit splitting.

For molecular species whose spectra showed no tunneling splitting, rotational transitions were fit using Pickett's SPFIT program[59]

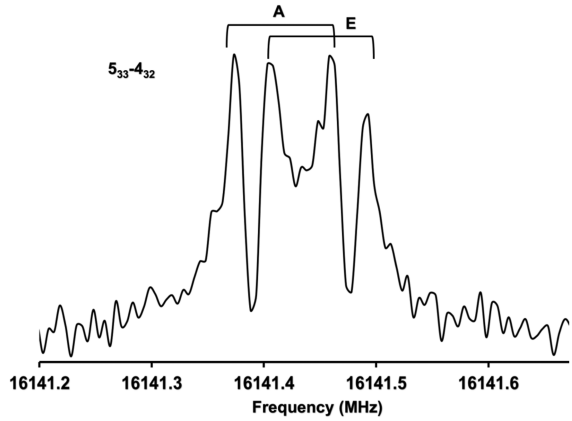

FIG. 4. A sample of the BF-FTMW spectrum showing the A/E splitting pattern due to the methyl internal rotation in conformer I in addition to the Doppler splitting of the instrument.

with Watson's A-reduced Hamiltonian[60] in the I^r representation to determine the experimental ground state rotational constants and centrifugal distortion constants. The results are provided in Tables II and III for the conformers and isotopologues of AES and AEE, respectively. For conformers I and II of AEE, the observed spectra were fit using the XIAM program,[61] which accounts for the methyl internal rotation using the combined axis method (CAM) and allows the derivation of key parameters for the molecule and the methyl rotor, including the V_3 barrier. This was done by assuming a value of the rotational constant of the methyl top (F_0) as well as the angle between the rotor a-axis and the principal inertial a-axis of the molecule (Δ) based on the theoretical geometry obtained from the B3LYP/D3(BJ)/aug-cc-PVTZ level of theory. The parameters determined in the fit are summarized in Table III and

TABLE II. Experimental spectroscopic parameters of AES for conformer I, including its ^{13}C and ^{34}S isotopologues, and conformer II.

	SPFIT							
Parameter	Conformer I	^{13}C1	^{13}C2	^{13}C3	^{34}S	^{13}C4	^{13}C5	Conformer II
A (MHz)[a]	3715.979 404(78)	3687.226 54(48)	3713.840 57(47)	3688.174 48(53)	3655.339 74(19)	3695.588 56(72)	3649.428 22(39)	4890.405 41(17)
B (MHz)	2038.353 451(57)	1994.359 65(84)	2011.430 17(82)	2029.041 56(92)	2028.022 20(18)	2021.854 2(12)	2014.128 93(49)	1621.808 257(76)
C (MHz)	1530.615 636(54)	1501.058 36(48)	1515.457 05(47)	1525.459 44(52)	1514.601 59(11)	1521.789 01(72)	1507.454 48(22)	1315.459 828(69)
Δ_J (kHz)[b]	2.276 46(72)	2.176(24)	2.202(24)	2.216(27)	2.180 2(24)	2.181(37)	2.323(13)	0.852 23(86)
Δ_{JK} (kHz)	−3.980 3(21)	−3.298(76)	−3.868(74)	−4.022(86)	−3.237(13)	−3.89(11)	−4.765(55)	−5.887 9(58)
Δ_K (kHz)	7.499 0(34)	6.588(65)	7.641(64)	7.743(72)	6.403(12)	7.395(85)	8.674(50)	21.231(17)
δ_J (kHz)	0.820 56(32)	0.773 8(98)	0.789 2(96)	0.799(11)	0.786 2(15)	0.780(15)	0.845 8(59)	0.266 99(50)
δ_K (kHz)	3.046 3(33)	3.23(24)	2.90(23)	2.68(25)	3.181(20)	2.52(34)	2.626(83)	1.359(15)
$\mu_a/\mu_b/\mu_c$[c]	y/y/y	y/y/n	y/y/n	y/y/n	y/y/n	y/y/n	y/y/n	y/y/y
N[d]	110	22	22	22	46	24	23	85
σ (kHz)[e]	1.2	0.9	0 .9	1.0	1.2	1.4	0.8	1.3

[a]Rotational constants.
[b]Quartic centrifugal distortion constants.
[c]Electric dipole moment components ("y" if observed and "n" if not observed).
[d]Total number of lines (N) in the fit.
[e]Root-mean-square error of the fit (σ). A complete list of the calculated rotational parameters at the B3LYP-D3(BJ)/aug-cc-pVTZ is given in Table S27.

TABLE III. Experimental spectroscopic parameters of AEE for conformer I, including its ^{13}C isotopologues, conformer II, and conformer III.

Parameter	XIAM Conformer I	SPFIT $^{13}C1$	SPFIT $^{13}C2$	SPFIT $^{13}C3$	SPFIT $^{13}C4$	SPFIT $^{13}C5$	XIAM Conformer II	SPFIT Conformer III
A (MHz)[a]	9469.242 34(37)	9297.716 51(46)	9453.457 16(50)	9322.084 86(49)	9429.012 37(45)	9396.649 93(49)	8444.667 06(55)	14 855.879 28(48)
B (MHz)	1724.233 22(8)	1694.485 29(12)	1700.414 37(14)	1721.645 52(16)	1708.890 34(13)	1684.768 59(13)	1754.760 66(12)	1389.648 74(11)
C (MHz)	1500.889 13(12)	1474.051 60(11)	1482.441 24(13)	1495.193 60(12)	1488.283 01(11)	1469.143 17(11)	1587.995 54(14)	1350.728 993(91)
Δ_J (kHz)[b]	0.275 68(69)	0.273 9(10)	0.265 1(13)	0.272 7(18)	0.268 8(11)	0.266 1(12)	0.863 1(11)	0.204 91(84)
Δ_{JK} (kHz)	−2.545 9(69)	−2.581(13)	−2.454(15)	−2.477(17)	−2.504(13)	−2.514(13)	−14.220 7(65)	−12.752(22)
Δ_K (kHz)	27.052(31)	[27.052]	[27.052]	[27.052]	[27.052]	[27.052]	102.29(11)	[371.092]
δ_J (kHz)	0.059 49(35)	0.063 9(12)	0.059 4(17)	0.061 1(15)	0.060 4(13)	0.059 4(13)	0.206 45(17)	−0.007 25(46)
δ_K (kHz)	0.719(28)	[0.719]	[0.719]	[0.719]	[0.719]	[0.719]	1.728(46)	[−1.363]
V_3 (kJ/mol)	12.172(55)						12.373(32)	
F_0 (GHz)	[160.291]						[160.309]	
Δ (rad)	[2.295]						[2.838]	
$\mu_a/\mu_b/\mu_c$[c]	y/y/n	y/y/n	y/y/n	y/y/n	y/y/n	y/y/n	y/y/y	y/y/n
N[d]	138	30	30	29	32	31	164	30
σ (kHz)[e]	2.9	1.1	1.3	1.2	1.2	1.2	2.9	1.1

[a]Rotational constants.
[b]Quartic centrifugal distortion constants.
[c]Electric dipole moment components ("y" if observed and "n" if not observed).
[d]Total number of lines (*N*) in the fit.
[e]Root-mean-square deviation of the fit (σ). The values in brackets for the isotopes were fixed to the conformer I values; for conformers I and II, to the values derived from theoretical molecular geometry obtained at the B3LYP-D3(BJ)/aug-cc-pVTZ level; and for conformer III, to the predicted values obtained at the same level of theory. A complete list of the calculated rotational parameters at the B3LYP-D3(BJ)/aug-cc-pVTZ level is given in Table S28.

compared with those derived from SPFIT (Table IV), where transitions within the two states (A/E) were treated separately. The complete line lists of the observed transition frequencies are given in Tables S29–S48, with the residuals (obs-calc) from the two fitting methods. Overall, the experimentally derived rotational and centrifugal distortion constants are in good agreement with their theoretical counterparts in Tables S27 and S28 of the electronic supplementary material. Furthermore, the internal rotation barriers

TABLE IV. Experimental spectroscopic parameters of AEE for conformer I and conformer II using SPFIT and XIAM.

Parameter	SPFIT Conformer I(A)	SPFIT Conformer I(E)	XIAM Conformer I	SPFIT Conformer II(A)	SPFIT Conformer II(E)	XIAM Conformer II
A (MHz)[a]	9469.242 63(48)	9469.243 4(12)	9469.242 34(37)	8444.667 09(47)	8444.668 7(23)	8444.667 06(55)
B (MHz)	1724.223 937(89)	1724.223 94(22)	1724.233 22(8)	1754.749 66(11)	1754.749 59(55)	1754.760 66(12)
C (MHz)	1500.898 35(14)	1500.898 63(34)	1500.889 13(12)	1588.006 53(13)	1588.006 57(62)	1587.995 54(14)
Δ_J (kHz)[b]	0.274 88(80)	0.276 8(20)	0.275 68(69)	0.863 2(10)	0.862 9(51)	0.863 1(11)
Δ_{JK} (kHz)	−2.538 3(80)	−2.541(20)	−2.545 9(69)	−14.220 1(59)	−14.227(29)	−14.220 7(65)
Δ_K (kHz)	26.902(36)	27.197(90)	27.052(31)	101.40(10)	103.24(50)	102.29(11)
δ_J (kHz)	0.059 81(41)	0.059 4(10)	0.059 49(35)	0.206 39(15)	0.206 47(75)	0.206 45(17)
δ_K (kHz)	0.723(33)	0.661(81)	0.719(28)	1.753(42)	1.72(21)	1.728(46)
V_3 (kJ/mol)			12.172(55)			12.373(32)
F_o (GHz)			[160.291]			[160.309]
Δ (rad)			[2.295]			[2.838]
$\mu_a/\mu_b/\mu_c$[c]	y/y/n	y/y/n	y/y/n	y/y/y	y/y/y	y/y/y
N[d]	69	69	138	82	82	164
σ (kHz)[e]	2.3	5.6	2.9	1.8	8.8	2.9

[a]Rotational constants.
[b]Quartic centrifugal distortion constants.
[c]Electric dipole moment components ("y" if observed and "n" if not observed).
[e]Total number of lines (*N*) in the fit.
[d]Root-mean-square deviation of the fit (σ). For conformers I and II, the values in the brackets were fixed to the values derived from theoretical molecular geometry obtained at the B3LYP-D3(BJ)/aug-cc-pVTZ level of theory.

of the methyl group for conformers I and II of AEE, 12.172(55) and 12.373(32) kJ mol^{-1}, respectively, are very similar to those from the B3LYP-D3(BJ)/aug-cc-pVTZ calculations (12.09 and 12.10 kJ mol^{-1}), which lends support to the assertion that methyl rotation is the origin of the observed splitting. This is similar to the V_3 barrier found in ethyl vinyl ether [12.85(10) kJ mol^{-1}][42] by analyzing rotational transitions in excited vibrational states when the ethyl adopts a comparable orientation relative to the bridging oxygen atom.

Structure determination

With rotational spectra observed for multiple isotopic species of the ground states of AEE and AES, their internal geometric parameters involving the heavy atoms were estimated using the experimental rotational constants given in Tables II and III. First, the positions of the substituted atoms were determined from Kraitchman's equations[62] as executed in Kisiel's KRA program.[63] The signs of the Kraitchman coordinates were deduced by comparing the positions of atoms in the equilibrium geometry (r_e) at the B3LYP-D3(BJ)/aug-cc-pVTZ level of theory, and the imaginary c-coordinate for oxygen in AEE was set to zero in the subsequent analysis as it lies in the ab-plane of the molecule. The results are given in Table S49 of the ESI. The atomic positions and their Costain errors[64] were then used to calculate the internal parameters of the r_s geometry using the EVAL routine,[63] and the results are summarized in Tables V and VI for both molecules. For AES, the r_e and r_s values for most parameters match to within two standard deviations with the exception of a few, r(C3–S), r(S–C4), and ∠C1–C2–C3–S, that depend on the position of sulfur, which is not well-determined due to its small c-coordinate (−0.086 28 ± 0.017 39 Å from Table S49). As the signal was not sufficient to observe transitions of ^{18}O for AEE, fewer parameters were determined in comparison with AES, but all derived values are within two standard deviations of the r_e values.

Next, the effective ground state geometries (r_0) of AES and AEE were derived using Kisiel's STRFIT program,[63] which performs a least squares fit of the selected geometric parameters to the moments of inertia of all observed isotopologues. For AES and AEE, 21 and 12 rotational constants were used in the fit, respectively. Since all of the heavy atoms in AEE are in the ab-plane (Fig. 5), the geometry was derived using only 2 rotational constants (A and B) for each isotopologue. The internal coordinates involving the hydrogen atoms for both AEE and AES (and oxygen in the case of AEE) were fixed to the computationally derived values at the B3LYP-D3(BJ)/aug-cc-pVTZ level of theory. The resulting r_0 parameters are summarized in Tables V and VI and, based on agreement with the

TABLE V. Equilibrium (r_e) (B3LYP/aug-cc-pVTZ), substitution (r_s), and ground state effective (r_0) structural parameters (bond lengths in Å; angles in deg) determined for AES.

	r_e	r_s	r_0
C1–C2	1.328	1.339(8)	1.343(8)
C2–C3	1.489	1.498(6)	1.482(10)
C3–S	1.841	1.810(8)	1.832(5)
S–C4	1.827	1.808(6)	1.796(5)
C4–C5	1.521	1.523(3)	1.536(8)
∠*C1–C2–C3*	124.3	123.0(7)	123.8(8)
∠*C3–S–C4*	101.0	100.8(1)	100.9(2)
∠*S–C4–C5*	114.5	114.3(5)	114.4(4)
∠*S–C3–C2*	112.1	112.6(5)	112.5(5)
∠*C1–C2–C3–S*	−113.2	−116.5(5)	−115.3(8)
∠*C2–C3–S–C4*	62.8	62.7(7)	63.3(5)
∠*C3–S–C4–C5*	69.3	69.8(6)	69.4(4)

TABLE VI. Equilibrium (r_e) (B3LYP/aug-cc-pVTZ), substitution (r_s), and ground state effective (r_0) structural parameters (bond lengths in Å; angles in deg) determined for AEE.

	r_e	r_s	r_0
C1–C2	1.325	1.328(7)	1.337(10)
C2–C3	1.494	1.505(6)	1.498(8)
C3–O	1.408	⋯	1.398(14)
O–C4	1.417	⋯	1.407(9)
C4–C5	1.513	1.514(4)	1.513(8)
∠*C1–C2–C3*	125.4	124.7(6)	124.7(4)
∠*C3–O–C4*	113.2	⋯	113.3(13)
∠*O–C3–C2*	111.3	⋯	111.2(6)
∠*O–C4–C5*	108.8	⋯	109.1(9)

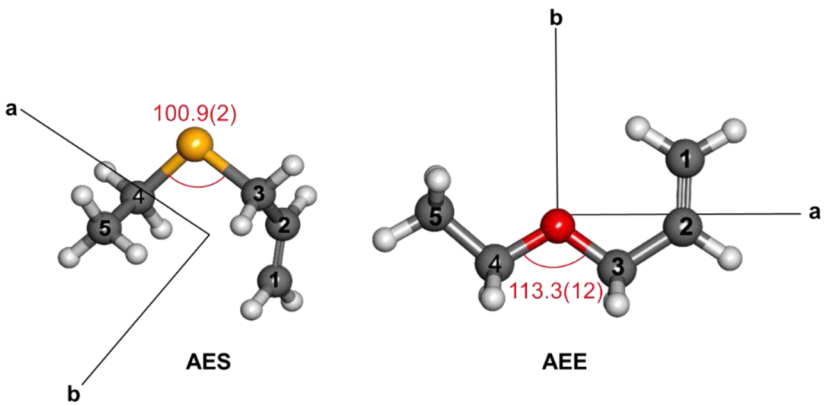

FIG. 5. Molecular geometries of conformers I of AES and AEE corresponding to the parameters in Tables V and VI.

theoretical predictions, provide confirmation that the assigned spectra arise from conformers I of AEE and AES. It is interesting to note that the bridging angle C–S–C (~101°) in the sulfide is smaller than the C–O–C angle (~113°) in AEE. This is analogous to what was reported in DAE and DAS[38] and is consistent with the hybridization of the bridging atoms identified from the NBO calculations,[58] with the C–S bonding orbitals on sulfur possessing a larger p-character (84%–85.03%) and favoring angles closer to those of atomic p-orbitals in AES compared to those on oxygen (72.2%–72.05%) in AEE, where the geometry at the center atom is closer to tetrahedral. This result confirms that hybridization models of bonding used to understand the molecular geometry of organic compounds that include second row elements (such as an sp^3 hybridized oxygen in this case) do not necessarily describe the bonding in heavier p-block elements.

DISCUSSION

Quantum chemical calculations predicted rich conformational landscapes for both AEE and AES arising from variations in the three dihedral angles that define the orientation of the organic fragments. In the jet-cooled rotational spectrum, the relative stabilities of the three lowest energy conformers of AEE and the two most stable conformers of AES were confirmed based on the observed spectral patterns that were consistent with the theoretical energy ordering. The absence of higher energy conformers is fairly common in jet-cooled studies, as it is well known that these can relax to lower energy geometries during the molecular beam expansion if the interconversion barrier is smaller than ~5 kJ mol^{-1}.[65] To further investigate the absence of conformer IV in AEE and conformer III in AES (as their relative energies indicate room temperature Boltzmann populations of around 9%–10%), potential relaxation pathways were calculated using systematic scans of the dihedral angles involved in the interconversion between these and lower energy conformers. Figure 6 shows the energy profile for the conversion of conformer III → II (barrier ~1.7 kJ mol^{-1}) of AES and conformer IV → I of AEE (barrier ~4.9 kJ mol^{-1}) by changing the λ and Φ dihedral angles (Fig. 1), respectively, while other parameters are relaxed. These barriers are sufficiently low to enable relaxation and explain the absence of transitions attributable to conformers III of AES and conformer IV of AEE in the rotational spectrum.

For AEE and AES, the computational results in Table I highlight a distinct difference from the earlier study of the related diallyl compounds,[38] as now, the S-bridged compound exists as a mixture of conformers at room temperature with three structures falling within a 5 kJ mol^{-1} energy window rather than one dominant form as in the earlier study of DAS. While it remains true that the lighter congener AEE still has the more competitive conformational equilibrium (as the conformers are more closely spaced energetically than for AES in Table I), the inclusion of an ethyl side chain has drastically altered the richness of the conformational equilibria for the S-bridged compound. Even more notable is that the predicted conformer geometries of AEE and AES are substantially different and surprisingly, this is even true for the lowest energy form (Fig. 1) in contrast to the case of DAE and DAS,[38] in which the organic groups were similarly oriented in the ground state structures. A closer inspection of the most stable structures in Fig. 1 shows that in AES, the allyl side chain is described by dihedral angles (θ and ϕ) of similar magnitude such that the conformers are largely differentiated by the orientation of the ethyl fragments (λ). The opposite dependence is seen in the lowest energy forms of AEE, with the ethyl groups adopting similar positions (λ) while the dihedral angles describing the allyl fragment (θ and ϕ) vary. The results of this comparison suggest that the bridging chalcogen atoms (oxygen vs sulfur) engage in unique interactions with saturated and unsaturated organic groups and that this key difference governs the conformational preferences of AEE and AES.

To identify possible non-covalent interactions that give rise to such distinct conformers of AES and AEE and to understand the underlying reasons for the energy ordering, we plotted isosurfaces of the reduced electron density gradient derived from NCI

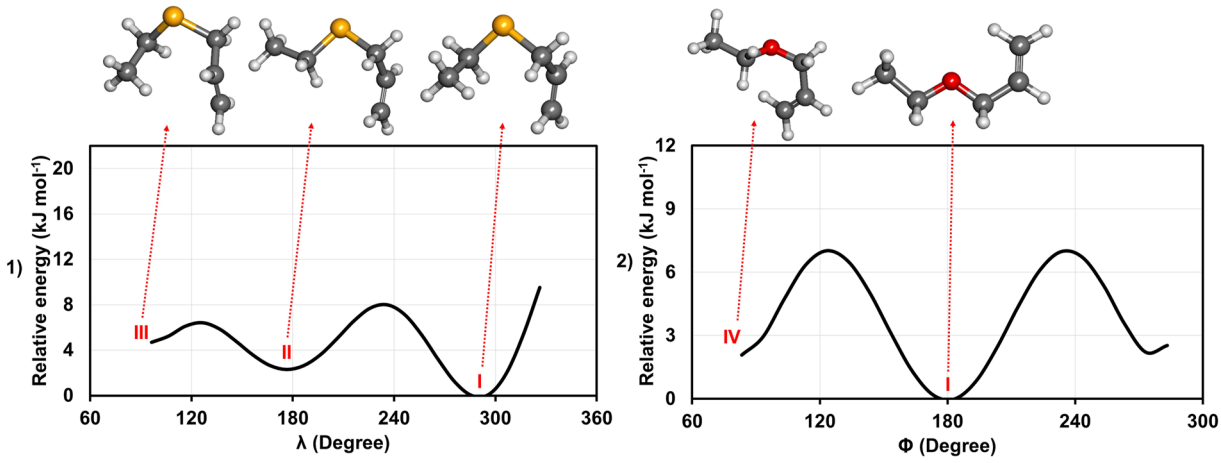

FIG. 6. Interconversion relaxation pathways (a) AES = III → II and (b) AEE = IV → I attained at the B3LYP-D3(BJ)/aug-cc-pVTZ level of theory.

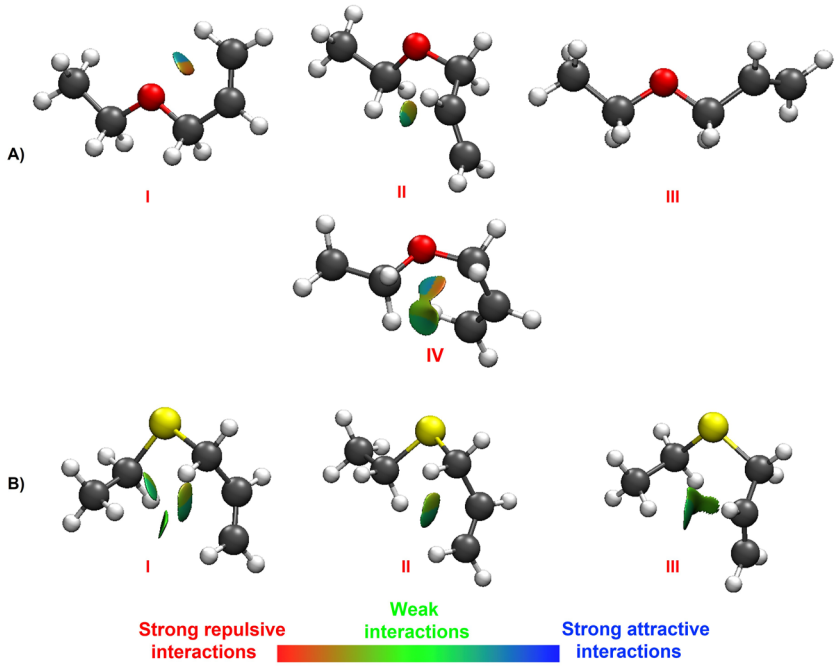

FIG. 7. NCI isosurfaces (s = 0.05, the color scale for $-0.02 < \rho < +0.02$ au) for (a) AEE conformers I–IV and (b) for conformers I–III of AES.

calculations.[57] For AEE, the results (Fig. 7) reveal blue-green and red regions that reflect the balance of attractive and repulsive interactions, respectively. In conformer I, the overall stabilizing influence seems to be due to attractive interactions between the terminal C–H bond of the allyl fragment and the oxygen atom (C–H···O), as seen by the blue isosurface appearing between these moieties. Similar interactions (C–H···N) were reported in the lower energy forms of diallyl amine (DAA)[22] and in a number of the low energy forms of DAE (although not the global minimum)[38] where the allyl group adopts an analogous orientation. For the remaining conformers of AEE and AES depicted in Fig. 7, it is difficult to predict the reason for the stability ordering due to the presence of largely green

TABLE VII. Select second-order perturbation energy for conformers I–III of AES and conformers I–IV of AEE with charge transfer interactions involving the lone pair (LP) on S and O. Figure 1 displays the labels for the atomic numbers, and the complete results are listed in ESI, Table S50.

AES interaction	Conformer I E (kJ/mol)	Conformer II E (kJ/mol)	Conformer III E (kJ/mol)
$LP_1(S) \rightarrow \sigma^* C_4–H'$	···	···	3.6
$LP_2(S) \rightarrow \sigma^* C_4–H$	···	16.6	5.8
$LP_2(S) \rightarrow \sigma^* C_4–H'$	14.8	16.7	3.1
$LP_1(S) \rightarrow \sigma^* C_5–C_4$	3.7	···	···
$LP_2(S) \rightarrow \sigma^* C_5–C_4$	17.4	···	20.6
$LP_2(S) \rightarrow \sigma^* C_5–H'$	3.6	···	4.2

AEE interaction	Conformer I E (kJ/mol)	Conformer II E (kJ/mol)	Conformer III E (kJ/mol)	Conformer IV E (kJ/mol)
$LP_1(O) \rightarrow \sigma^* C_3–C_2$	5.4	3.3	4.6	2.5
$LP_2(O) \rightarrow \sigma^* C_3–C_2$	···	27.2	···	4.7
$LP_2(O) \rightarrow \pi^* C_2–C_1$	···	4.9	···	3.8
$LP_1(O) \rightarrow \sigma^* C_3–H$	3	4.9	3.1	···
$LP_1(O) \rightarrow \sigma^* C_3–H'$	3	11.1	···	···
$LP_2(O) \rightarrow \sigma^* C_3–H$	28.6	27.2	25.1	10
$LP_2(O) \rightarrow \sigma^* C_3–H'$	28.6	···	29.6	7.3

isosurfaces, which indicate a combination of weak contacts between different bonds or atoms that can be either net attractive or repulsive interactions (referring to the color-coded scale in Fig. 7). In such cases, second-order perturbation energies from NBO analyses can help identify specific orbital interactions and their relative importance in stabilizing the conformer.

The stabilizing interactions identified via NBO analysis are provided as the supplementary material in Table S50, and a shorter summary is provided in Table VII to highlight some key interactions involving the lone pair (LP) electron density on sulfur and oxygen. For AES, for example, there are no significant differences in the intramolecular contacts between sulfur and the allyl fragment (Table S50) for the three stable conformers. This is consistent with the θ and Φ dihedral angles being similar for all three; however, note that conformer III differs from the other two in the signs of both θ and ϕ, but the magnitude is comparable. This orientation of the allyl fragment is also observed for the most stable geometries of both DAE and DAS, where both side chains point downward, and was found to facilitate charge transfer of LP electron density from the chalcogen to the π^* orbital of the C=C bond. Maintaining the stability offered by this orientation of the allyl group, the relative energies of conformers I through III are then dependent on LP donation from sulfur into the C–C bond [LP(S) → σ^* C_5–C_4] and neighboring methylene C–H bonds [LP(S) → σ^*C_4–H] of the ethyl fragment. The corresponding second-order perturbation energies for these interactions, which vary with λ (i.e., the orientation of ethyl), are summarized in Table VII for AES.

Interestingly, as noted earlier, the ethyl side chains in the most stable conformers of AEE are positioned similarly and it is the unique interactions between the LP electron density on oxygen and the allyl fragments that influence the relative energies of the first four conformers. In this case, the conformational equilibrium is very competitive, as seen by the similar energies in Table I, and thus, it is difficult to pinpoint a specific interaction or set of interactions that give rise to this energy ordering. The overall ordering is, instead, a balance of many subtle effects, of which only a small subset involving the allyl fragment is included in Table VII in AEE. In comparing the NBO results for AEE and AES, the overarching trend appears to be that it is the bridging atom's LP interactions with the saturated side chains that are most important for defining the relative stability of conformers in the sulfide and with the (partially) unsaturated group in the case of the ether. It would be interesting to extend this to other side chains, and in fact, we are currently pursuing several other examples to test the universality of this finding.

CONCLUSIONS

The conformational equilibria of AEE and AES were characterized using quantum chemical calculations and Fourier transform microwave spectroscopy. Rotational transitions consistent with the three lowest energy forms of AEE and the two most stable conformers of AES were assigned. A tunneling splitting in the high resolution spectra of conformers I and II of AEE was attributed to methyl internal rotation and used to derive the corresponding V_3 barriers that were consistent with theoretical predictions. The results of this study highlight the dramatic differences in the stability of various conformers of AEE and AES upon replacing the bridging atom from oxygen to sulfur. The experimentally derived structural parameters for the ground state conformers of AEE and AES revealed that the C–X–C angle is 12° smaller in the latter due to the greater p-orbital character of bonding orbitals on sulfur. More surprising, however, are the distinct orientations of organic side chains in the ether vs sulfide species. Based on NBO calculations, this appears to arise from stabilizing orbital interactions involving the lone pair electron density on the bridging atom. For AEE, it is the unique LP(O) donation to the allyl fragment that drives the energy ordering of the lowest conformers, while it is the differences in the LP(S) donation to the ethyl group that define the relative stabilities in AES. The results presented here for AEE and AES highlight the subtle but critically important nature of intramolecular interactions that stabilize distinct geometries of organic ethers and sulfides. The surprising variability in the relative energies and shapes of these organochalcogens reaffirms the role that rotational spectroscopy and quantum chemistry play in informing improved models of bonding, structure, and dynamics that may inspire the design of novel compounds with desirable functional properties.

SUPPLEMENTARY MATERIAL

Appendix 1: Cartesian coordinates for the energy minima of AES and AEE. **Appendix 2**: Calculated energetic and spectroscopic parameters for conformers I and II of AES and conformers I–III of AEE. **Appendix 3**: Assigned transitions for the observed species of conformers I and II of AES and conformers I–III of AEE. **Appendix 4:** Kraitchman coordinates of conformer I of AES and AEE. **Appendix 5:** NBO analysis for conformers I–III of AES and conformers I–IV of AEE.

ACKNOWLEDGMENTS

This research was funded by the Natural Sciences and Engineering Research Council of Canada (NSERC) through the Discovery Grant program and the high performance computing facility (GREX) provided by the University of Manitoba and Digital Research Alliance of Canada (formerly Compute Canada). T.P. was supported by the Faculty of Graduate studies through a UM graduate fellowship.

AUTHOR DECLARATIONS

Conflict of Interest

The authors have no conflicts to disclose.

Author Contributions

Tamanna Poonia: Conceptualization (lead); Data curation (lead); Formal analysis (lead); Investigation (lead); Methodology (lead); Writing – original draft (lead); Writing – review & editing (supporting). **Jennifer van Wijngaarden**: Data curation (equal); Funding acquisition (lead); Project administration (lead); Resources (lead); Supervision (lead); Writing – original draft (equal); Writing – review & editing (lead).

DATA AVAILABILITY

The data that support the findings of this study are available within the article and its supplementary material.

REFERENCES

[1] G. C. Hoover and D. S. Seferos, "Photoactivity and optical applications of organic materials containing selenium and tellurium," Chem. Sci. **10**(40), 9182–9188 (2019).

[2] I. F. Perepichka, D. F. Perepichka, H. Meng, and F. Wudl, "Light-emitting polythiophenes," Adv. Mater. **17**(19), 2281–2305 (2005).

[3] Y. Li and Y. Zou, "Conjugated polymer photovoltaic materials with broad absorption band and high charge carrier mobility," Adv. Mater. **20**(15), 2952–2958 (2008).

[4] T. P. Kaloni, P. K. Giesbrecht, G. Schreckenbach, and M. S. Freund, "Polythiophene: From fundamental perspectives to applications," Chem. Mater. **29**(24), 10248–10283 (2017).

[5] M. C. Iovu, E. E. Sheina, R. R. Gil, and R. D. McCullough, "Experimental evidence for the quasi-'living' nature of the grignard metathesis method for the synthesis of regioregular poly(3-alkylthiophenes)," Macromolecules **38**(21), 8649–8656 (2005).

[6] Z. Lou, P. Li, and K. Han, "Redox-responsive fluorescent probes with different design strategies," Acc. Chem. Res. **48**(5), 1358–1368 (2015).

[7] T. Gneuß, M. J. Leitl, L. H. Finger, N. Rau, H. Yersin, and J. Sundermeyer, "A new class of luminescent Cu(I) complexes with tripodal ligands-TADF emitters for the yellow to red color range," Dalton Trans. **44**(18), 8506–8520 (2015).

[8] Y. Yamashita, "Organic semiconductors for organic field-effect transistors," Sci. Technol. Adv. Mater. **10**(2), 024313 (2009).

[9] J. G. Manion, J. R. Panchuk, and D. S. Seferos, "Applying heteroatom substitution in organic photovoltaics," Chem. Rec. **19**(6), 1113–1122 (2019).

[10] S. Ye, L. Janasz, W. Zajaczkowski, J. G. Manion, A. Mondal, T. Marszalek, D. Andrienko, K. Müllen, W. Pisula, and D. S. Seferos, "Self-organization and charge transport properties of selenium and tellurium analogues of polythiophene," Macromol. Rapid Commun. **40**(1), 1800596 (2019).

[11] E. L. Kynaston, K. J. Winchell, P. Y. Yee, J. G. Manion, A. D. Hendsbee, Y. Li, S. Huettner, S. H. Tolbert, and D. S. Seferos, "Poly(3-alkylthiophene)- block-poly(3-alkylselenophene)s: Conjugated diblock co-polymers with atypical self-assembly behavior," ACS Appl. Mater. Interfaces **11**(7), 7174–7183 (2019).

[12] M. Jeffries-El, B. M. Kobilka, and B. J. Hale, "Optimizing the performance of conjugated polymers in organic photovoltaic cells by traversing group 16," Macromolecules **47**(21), 7253–7271 (2014).

[13] E. L. Kynaston, Y. Fang, J. G. Manion, N. K. Obhi, J. Y. Howe, D. F. Perepichka, and D. S. Seferos, "Patchy nanofibers from the thin film self-assembly of a conjugated diblock copolymer," Angew. Chem. **129**(22), 6248–6252 (2017).

[14] A. Breder and S. Ortgies, "Recent developments in sulfur- and selenium-catalyzed oxidative and isohypsic functionalization reactions of alkenes," Tetrahedron Lett. **56**(22), 2843–2852 (2015).

[15] T. Nishiguchi, Y. Yoshikawa, and H. Yasui, "Anti-diabetic effect of organochalcogen (sulfur and selenium) zinc complexes with hydroxy-pyrone derivatives on leptin-deficient type 2 diabetes model ob/ob mice," Int. J. Mol. Sci. **18**(12), 2647 (2017).

[16] D. De Souza, D. O. C. Mariano, F. Nedel, E. Schultze, V. F. Campos, F. Seixas, R. S. Da Silva, T. S. Munchen, V. Ilha, L. Dornelles, A. L. Braga, J. B. T. Rocha, T. Collares, and O. E. D. Rodrigues, "New organochalcogen multitarget drug: Synthesis and antioxidant and antitumoral activities of chalcogenozidovudine derivatives," J. Med. Chem. **58**(8), 3329–3339 (2015).

[17] F. Penteado, B. Monti, L. Sancineto, G. Perin, R. G. Jacob, C. Santi, and E. J. Lenardão, "Ultrasound-assisted multicomponent reactions, organometallic and organochalcogen chemistry," Asian J. Org. Chem. **7**(12), 2368–2385 (2018).

[18] P. Oswal, A. Arora, S. Singh, D. Nautiyal, S. Kumar, G. K. Rao, and A. Kumar, "Organochalcogen ligands in catalysis of oxidation of alcohols and transfer hydrogenation," Dalton Trans. **49**(36), 12503–12529 (2020).

[19] A. Kirchhain, W. Yu, and L. Engman, "Organochalcogen stabilizers efficiently protect model polyolefins exposed to chlorinated media," Polym. Degrad. Stab. **118**, 82–87 (2015).

[20] I. C. Mondal, M. Galkin, S. Sharma, N. A. Murugan, D. A. Yushchenko, K. Girdhar, A. Karmakar, P. Mondal, P. Gaur, and S. Ghosh, "Organosulfur/selenium-based highly fluorogenic molecular probes for live-cell nucleolus imaging," Chem. - Asian J. **17**(7), e2021012 (2022).

[21] W. G. D. P. Silva, T. Poonia, and J. Wijngaarden, "Targeting the rich conformational landscape of *N*-allylmethylamine using rotational spectroscopy and quantum mechanical calculations," ChemPhysChem **21**(22), 2515–2522 (2020).

[22] W. G. D. P. Silva, G. Daudet, S. Perez, S. Thorwirth, and J. van Wijngaarden, "Conformational preferences of diallylamine: A rotational spectroscopic and theoretical study," J. Chem. Phys. **154**(16), 1–25 (2021).

[23] J. Stitsky, W. G. D. P. Silva, W. Sun, and J. Van Wijngaarden, "Conformers of allyl isothiocyanate: A combined microwave spectroscopy and computational study," J. Phys. Chem. A **124**(19), 3876–3885 (2020).

[24] W. G. D. P. Silva, T. Poonia, and J. van Wijngaarden, "Exploring the non-covalent interactions behind the formation of amine-water complexes: The case of *N*-allylmethylamine monohydrate," Phys. Chem. Chem. Phys. **23**(12), 7368–7375 (2021).

[25] F. Xie, S. Mahendiran, N. A. Seifert, and Y. Xu, "Modifying conformational distribution of chiral tetrahydro-2-furoic acid through its interaction with water: A rotational spectroscopic and theoretical investigation," Phys. Chem. Chem. Phys. **23**(6), 3820–3825 (2021).

[26] A. M. Rijs, B. O. Crews, M. S. de Vries, J. S. Hannam, D. A. Leigh, M. Fanti, F. Zerbetto, and W. J. Buma, "Shaping of a conformationally flexible molecular structure for spectroscopy," Angew. Chem. **120**(17), 3218–3223 (2008).

[27] S. R. Domingos, C. Pérez, C. Medcraft, P. Pinacho, and M. Schnell, "Flexibility unleashed in acyclic monoterpenes: Conformational space of citronellal revealed by broadband rotational spectroscopy," Phys. Chem. Chem. Phys. **18**(25), 16682–16689 (2016).

[28] M. Fatima, D. Maué, C. Pérez, D. S. Tikhonov, D. Bernhard, A. Stamm, C. Medcraft, M. Gerhards, and M. Schnell, "Structures and internal dynamics of diphenylether and its aggregates with water," Phys. Chem. Chem. Phys. **22**(48), 27966–27978 (2020).

[29] A. Mardyukov, H. Quanz, and P. R. Schreiner, "Conformer-specific hydrogen atom tunnelling in trifluoromethylhydroxycarbene," Nat. Chem. **9**(1), 71–76 (2017).

[30] C. Cabezas, J.-C. Guillemin, and Y. Endo, "Conformational analysis of ethyl-substituted Criegee intermediate by FTMW spectroscopy," J. Chem. Phys. **145**(22), 224314 (2016).

[31] P. Vansteenkiste, E. Pauwels, V. Van Speybroeck, and M. Waroquier, "Rules for generating conformers and their relative energies in *n*-alkanes with a heteroelement O or S: Ethers and alcohols, or sulfides and thiols," J. Phys. Chem. A **109**(42), 9617–9626 (2005).

[32] R. E. Schmidt and C. R. Quade, "Microwave spectrum of ethyl mercaptan," J. Chem. Phys. **62**, 3864–3874 (1975).

[33] J. Nakagawa and M. Hayashi, "Internal rotation in propyl mercaptan by microwave spectroscopy," J. Mol. Spectrosc. **85**(2), 327–340 (1981).

[34] Y. Kawashima, Y. Tanaka, T. Uzuyama, and E. Hirota, "Conformations and low-frequency intramolecular motions of 1-butanol, 1-butanethiol, iso-butanol, and iso-butanethiol investigated by fourier transform microwave spectroscopy combined with quantum chemical calculations," J. Phys. Chem. A **125**(5), 1166–1183 (2021).

[35] M. Takano, Y. Sasada, and T. Satoh, "Microwave spectrum of ethyl alcohol: The trans rotamer," J. Mol. Spectrosc. **26**(2), 157–162 (1968).

[36] A. Maeda, F. C. De Lucia, E. Herbst, J. C. Pearson, J. Riccobono, E. Trosell, and R. K. Bohn, "The millimeter- and submillimeter-wave spectrum of the *Gt* conformer of *n*-propanol (*n*-$CH_3CH_2CH_2OH$)," Astrophys. J. Suppl. Ser. **162**(2), 428–435 (2006).

[37] Z. Kisiel, O. Dorosh, A. Maeda, I. R. Medvedev, F. C. De Lucia, E. Herbst, B. J. Drouin, J. C. Pearson, and S. T. Shipman, "Determination of precise relative energies of conformers of *n*-propanol by rotational spectroscopy," Phys. Chem. Chem. Phys. **12**(29), 8329–8339 (2010).

[38] T. Poonia, W. G. D. P. Silva, and J. van Wijngaarden, "Dramatic differences in the conformational equilibria of chalcogen-bridged compounds: The case of

diallyl ether versus diallyl sulfide," Phys. Chem. Chem. Phys. **24**(1), 240–248 (2022).
[39]W. Caminati, A. C. Fantoni, C. Paolucci, and B. Velino, "Conformational equilibrium in methyl allyl ether," J. Mol. Spectrosc. **145**(2), 362–370 (1991).
[40]A. C. Fantoni, "Microwave spectrum, conformation rotation in allyl methyl sulfide," J. Mol. Struct. **243**, 131–139 (1991).
[41]P. Cahill, L. P. Gold, and N. L. Owen, "Microwave spectrum, conformation, dipole moment, and barrier to internal rotation in methyl vinyl ether," J. Chem. Phys. **48**(4), 1620–1626 (1968).
[42]N. L. Owen and G. O. Soerensen, "Microwave spectrum, conformation, internal and barrier to rotation of ethyl vinyl ether," J. Phys. Chem. **83**(11), 1483–1488 (1979).
[43]F. Weinhold, C. R. Landis, and E. D. Glendening, "What is NBO analysis and how is it useful?," Int. Rev. Phys. Chem. **35**(3), 399–440 (2016).
[44]E. R. Johnson, S. Keinan, P. Mori-Sánchez, J. Contreras-García, A. J. Cohen, and W. Yang, "Revealing noncovalent interactions," J. Am. Chem. Soc. **132**(18), 6498–6506 (2010).
[45]G. G. Brown, B. C. Dian, K. O. Douglass, S. M. Geyer, and B. H. Pate, "The rotational spectrum of epifluorohydrin measured by chirped-pulse Fourier transform microwave spectroscopy," J. Mol. Spectrosc. **238**(2), 200–212 (2006).
[46]T. J. Balle and W. H. Flygare, "Fabry-Perot cavity pulsed Fourier transform microwave spectrometer with a pulsed nozzle particle source," Rev. Sci. Instrum. **52**(1), 33–45 (1981).
[47]L. Evangelisti, G. Sedo, and J. van Wijngaarden, "Rotational spectrum of 1,1,1-trifluoro-2-butanone using chirped-pulse Fourier transform microwave spectroscopy," J. Phys. Chem. A **115**(5), 685–690 (2011).
[48]G. Sedo and J. van Wijngaarden, "Fourier transform microwave spectra of a 'new' isomer of OCS-CO_2," J. Chem. Phys. **131**(4), 044303 (2009).
[49]C. Bannwarth, S. Ehlert, and S. Grimme, "GFN2-xTB—An accurate and broadly parametrized self-consistent tight-binding quantum chemical method with multipole electrostatics and density-dependent dispersion contributions," J. Chem. Theory Comput. **15**(3), 1652–1671 (2019).
[50]S. Grimme, "Exploration of chemical compound, conformer, and reaction space with meta-dynamics simulations based on tight-binding quantum chemical calculations," J. Chem. Theory Comput. **15**(5), 2847–2862 (2019).
[51]P. Pracht, F. Bohle, and S. Grimme, "Automated exploration of the low-energy chemical space with fast quantum chemical methods," Phys. Chem. Chem. Phys. **22**(14), 7169–7192 (2020).
[52]A. D. Becke, "A new inhomogeneity parameter in density-functional theory," J. Chem. Phys. **109**(6), 2092–2098 (1998).
[53]S. Grimme, S. Ehrlich, and L. Goerigk, "Effect of the damping function in dispersion corrected density functional theory," J. Comput. Chem. **32**(7), 1456–1465 (2011).
[54]S. Grimme, J. Antony, S. Ehrlich, and H. Krieg, "A consistent and accurate *ab initio* parametrization of density functional dispersion correction (DFT-D) for the 94 elements H-Pu," J. Chem. Phys. **132**(15), 154104 (2010).
[55]T. H. Dunning, "Gaussian basis sets for use in correlated molecular calculations. I. The atoms boron through neon and hydrogen," J. Chem. Phys. **90**(2), 1007–1023 (1989).
[56]M. J. Frisch, G. W. Trucks, H. B. Schlegel, G. E. Scuseria, M. A. Robb, J. R. Cheeseman, G. Scalmani, V. Barone, B. Mennucci, G. A. Petersson, H. Nakatsuji, M. Caricato, X. Li, H. P. Hratchian, A. F. Izmaylov, J. Bloino, G. Zheng, J. L. Sonnenberg, M. Hada, M. Ehara, K. T. R. Fukuda, J. Hasegawa, M. Ishida, T. Nakajima, Y. Honda, O. Kitao, H. Nakai, T. Vreven, J. A. Montgomery, J. E. Peralta, F. Ogliaro, M. Bearpark, J. J. Heyd, E. Brothers, K. N. Kudin, V. N. Staroverov, R. Kobayashi, J. Normand, K. Raghavachari, A. Rendell, J. C. Burant, S. S. Iyengar, J. Tomasi, M. Cossi, N. Rega, J. M. Millam, M. Klene, J. E. Knox, J. B. Cross, V. Bakken, C. Adamo, J. Jaramillo, R. Gomperts, R. E. Stratmann, O. Yazyev, A. J. Austin, R. Cammi, C. Pomelli, J. W. Ochterski, R. L. Martin, K. Morokuma, V. G. Zakrzewski, G. A. Voth, P. Salvador, J. J. Dannenberg, S. Dapprich, A. D. Daniels, Farkas, J. B. Foresman, J. V Ortiz, J. Cioslowski, and D. J. Fox, Gaussian 16 (Revision C.01), Gaussian, Inc., Wallingford, CT, 2016.
[57]J. Contreras-García, E. R. Johnson, S. Keinan, R. Chaudret, J. P. Piquemal, D. N. Beratan, and W. Yang, "NCIPLOT: A program for plotting noncovalent interaction regions," J. Chem. Theory Comput. **7**(3), 625–632 (2011).
[58]E. D. Glendening, J. K. Badenhoop, A. E. Reed, J. E. Carpenter, J. A. Bohmann, C. M. Morales, P. Karafiloglou, C. R. Landis, and F. Weinhold, NBO 7.0, Theoretical Chemistry Institute, University of Wisconsin, Madison, 2018.
[59]H. M. Pickett, "The fitting and prediction of vibration-rotation spectra with spin interactions," J. Mol. Spectrosc. **148**(2), 371–377 (1991).
[60]J. K. G. Watson, "Determination of centrifugal distortion coefficients of asymmetric-top molecules. III. Sextic coefficients," J. Chem. Phys. **48**(10), 4517–4524 (1968).
[61]H. Hartwig and H. Dreizler, "The microwave spectrum of trans-2,3-dimethyloxirane in torsional excited states," Z. Nat., Sect. A **51**(8), 923–932 (1996).
[62]J. Kraitchman, "Determination of molecular structure from microwave spectroscopic sata," Am. J. Phys. **21**(1), 17–24 (1953).
[63]Z. Kisiel, *Spectroscopy from Space* (Kluwer Academic Publishers, 2001), pp. 91–106.
[64]C. C. Costain, "Further comments on the accuracy of R substitution structures," Trans. Am. Crystallogr. Assoc. **2**, 157–164 (1966).
[65]R. S. Ruoff, T. D. Klots, T. Emilsson, and H. S. Gutowsky, "Relaxation of conformers and isomers in seeded supersonic jets of inert gases," J. Chem. Phys. **93**(5), 3142–3150 (1990).